Available online at www.sciencedirect.com

ScienceDirect

Mendeleev Commun., 2024, **34**, 484–487

Mendeleev Communications

Synthesis, structure, and photoluminescent properties of a mixed carboxylate pentafluorobenzoate–phenylacetate complex of terbium

Natalia V. Gogoleva,*[a] Maxim A. Shmelev,[a] Aleksandr S. Chistyakov,[a] Galina A. Razgonyaeva,[a] Vladislav M. Korshunov,[b] Alisia V. Tsorieva,[b] Ilya V. Taydakov,[b] Alexey A. Sidorov[a] and Igor L. Eremenko[a]

[a] *N. S. Kurnakov Institute of General and Inorganic Chemistry, Russian Academy of Sciences, 119991 Moscow, Russian Federation. E-mail: judiz@rambler.ru*

[b] *P. N. Lebedev Physical Institute, Russian Academy of Sciences, 119991 Moscow, Russian Federation*

DOI: 10.1016/j.mencom.2024.06.005

A complex of mixed carboxylate pentafluorobenzoate (pfb) and phenylacetate (PhAc), *viz.* $[Tb_2(phen)_2(pfb)_2(PhAc)_4]$ (phen is 1,10-phenanthroline), where each rare earth element (REE) ion is simultaneously coordinated to pentafluorobenzoic and phenylacetic acid anions, was for the first time synthesized and structurally characterized. To evaluate the influence of the second type of anion on the structure and photoluminescent properties, compounds with phenylacetic acid anions $[Tb_2(phen)_2(PhAc)_6]$ and pentafluorobenzoic acid anions $[Tb_2(EtOH)_2(phen)_2(pfb)_6]$ were obtained. A change in the composition of the compounds from the phenylacetic acid anion to pentafluorobenzoate led to a change in the geometry of the metal scaffold and the REE polyhedron, a rearrangement of the system of non-covalent interactions according to the Hirshfeld surface analysis, and enhanced luminescence.

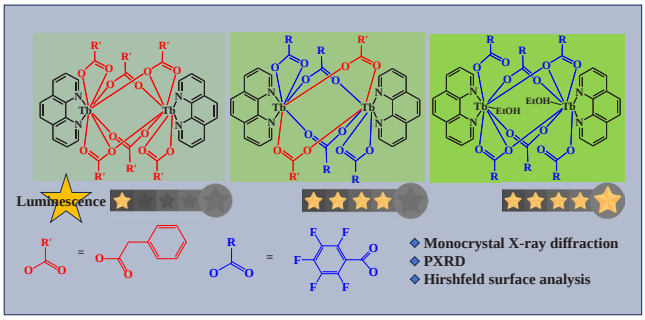

Keywords: terbium^{3+}, mixed carboxylate complexes, X-ray structure, non-covalent interactions, Hirshfeld surface analysis, photoluminescence.

A combination of several ligands within lanthanide complexes can lead to a structural modification and improvement of their luminescent characteristics by varying the geometry of metal ion coordination polyhedra, minimizing interionic interactions, and reducing conformational mobility.[1–8] Using europium compounds as an example, Lima *et al.*[9] demonstrated that the simultaneous combination of four anionic ligands in a complex can result in a fivefold increase in luminescent efficiency. A samarium complex with four anionic ligands had a record quantum yield of luminescence for this metal ion.[10] However, the above compounds have not been structurally characterized with a detailed investigation into the influence of the simultaneous coordination of multiple anionic fragment types on the structure of complexes with lanthanide ions.

In this work, we studied the structure and photoluminescent characteristics of a mixed carboxylate complex with Tb^{3+} ions and the anions of pentafluorobenzoic acid, phenylacetic acid, and 1,10-phenanthroline. The combination of both fluorinated carboxylic acid anions and aromatic ligands in the complex led to the formation of additional non-covalent interactions between aromatic fragments of the ligands (π···π, C–F···π, and C–H···F), which can significantly influence the structure and crystalline packing of the resulting complexes.[11–18] The phenylacetate substituent, due to its methylene linker, exhibits greater mobility compared to the phenyl group, potentially affecting the structure of mixed carboxylate compounds and stabilizing the crystal lattice through increased participation in intermolecular interactions.[19]

When terbium(III) acetate interacted with a mixture of pentafluorobenzoic acid H(pfb) and phenylacetic acid H(PhAc) in the presence of 1,10-phenanthroline (phen) in ethanol, the heteroanionic complex $[Tb_2(phen)_2(pfb)_4(PhAc)_2]$ (**1**) was formed (Scheme 1). In this complex, each rare earth element (REE) ion simultaneously coordinates the anions of both pentafluorobenzoic and phenylacetic acids. When varying the ratio of the starting reagents $[Tb(OAc)_3$: H(pfb) : H(PhAc) = 1 : 2 : 1 or 1 : 1 : 2], no mixed carboxylate complexes with a different ratio of PhAc/pfb anions crystallized, and only complex **1** was formed. Additionally, to study the influence of the second anion type on the photoluminescent properties of complex **1**, new compounds $[Tb_2(phen)_2(PhAc)_6]$ (**2**) and $[Tb_2(EtOH)_2(phen)_2(pfb)_6]$ (**3**) were obtained with phenylacetic and pentafluorobenzoic acid anions, respectively (Scheme 1). The structures of compounds **1**–**3** were investigated using the X-ray diffraction analysis.[†] The

[†] Single-crystal X-ray diffraction analysis of compounds **1**–**3** was performed on a Bruker D8 Venture diffractometer equipped with a CCD detector (MoKα, λ = 0.71073 Å; CuKα, λ = 1.54178 Å, graphite monochromator). A semi-empirical absorption correction using the SADABS[20] program was applied to all compounds. Using Olex2,[21] the structure was solved with the ShelXS structure solution program using direct methods and refined using the ShelXL[22] refinement package with the least squares minimization in anisotropic approximation

$$Tb(OAc)_3{\cdot}5H_2O + H(pfb) + 2H(PhAc) + phen{\cdot}H_2O \xrightarrow{MeCN,\ EtOH} [Tb_2(phen)_2(pfb)_4(PhAc)_2]$$
1

$$Tb(OAc)_3{\cdot}5H_2O + 2H(pfb) + H(PhAc) + phen{\cdot}H_2O \xrightarrow{MeCN,\ EtOH} [Tb_2(phen)_2(pfb)_4(PhAc)_2]$$
1

$$Tb(OAc)_3{\cdot}5H_2O + 3H(PhAc) + phen{\cdot}H_2O \xrightarrow{EtOH} [Tb_2(phen)_2(PhAc)_6]$$
2

$$Tb(H_2O)_4(pfb)_3 + phen{\cdot}H_2O \xrightarrow{EtOH} [Tb_2(EtOH)_2(phen)_2(pfb)_2]$$
3

Scheme 1

main bond lengths and angles are given in Table S1 (see Online Supplementary Materials). The phase purity of the complexes was confirmed by X-ray powder diffraction (Figures S1–S3) and CHN analyses.

In the structure of binuclear complex **1**, Tb^{3+} ions are coordinated by two bridging pfb anions and two bridging PhAc anions (Figure 1). Each Tb^{3+} ion completes its coordination environment to form a square antiprism [TbN_2O_6, CShM(Tb) = 1.179] by coordinating with two oxygen atoms from pentafluorobenzoic acid and two nitrogen atoms from phenanthroline in the equatorial plane. In the structure of complex **1**, the formation of a stable fragment {$Tb_2(phen)_2(pfb)_2$} was observed, in which π···π and C–F···π interactions between the pfb anion and the phenanthroline molecule (Tables S2, S3) stabilize such a molecular geometry (Figure 1).

The crystalline packing of **1** was formed through multiple intermolecular stacking interactions between fluorinated and non-fluorinated aromatic fragments. Contacts between chelating

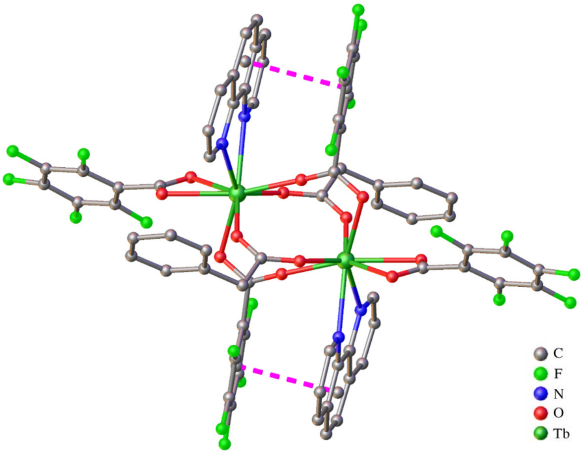

Figure 1 Structure of complex **1**. Intramolecular stacking interactions are indicated by dashed lines; hydrogen atoms are not shown.

anions of pentafluorobenzoic acid and phenylacetate anions and interactions between pairs of phenanthroline molecules were present (Figure S4, Table S2). Additionally, C–F···π and C–H···F interactions contributed to the stabilization of the packing with the formation of a supramolecular framework structure (Figure S4 and Tables S2, S3).

In the structure of complex **2** (Figure 2), metal ions were coordinated by two bridging and two chelating bridging PhAc anions. Each metal ion completed its coordination environment to form a 'muffin' polyhedron by coordinating with two oxygen atoms of the chelating bound PhAc anion and two nitrogen atoms of phenanthroline [CShM(Tb) = 1.664]. The main structural difference between heteroanionic complex **1** and homoanionic complex **2** lies in the arrangement of phenanthroline molecules: in complex **1**, they are located in the equatorial plane, while they act as axial ligands in **2**.

The crystal packing of compound **2** was stabilized by intermolecular stacking interactions between pairs of phen molecules, forming a supramolecular chain parallel to the *a* axis (Table S2). The oxygen atoms of the PhAc anions were involved in multiple C–H···O interactions with the hydrogen atoms of phen molecules, creating a supramolecular layer (Table S4).

In the structure of complex **3**, metal ions were bridged by two bridging and two chelating bridging pfb anions (Figure 3). Each Tb^{3+} ion completed its coordination environment to form a 'muffin' polyhedron through the coordination of phen, EtOH, and monodentate bound pfb anion [CShM(Tb) = 1.337]. Similarly to compound **1**, the formation of π···π and C–F···π interactions between the pfb anion and the phen molecule was observed in the equatorial plane of complex **3**. However, the

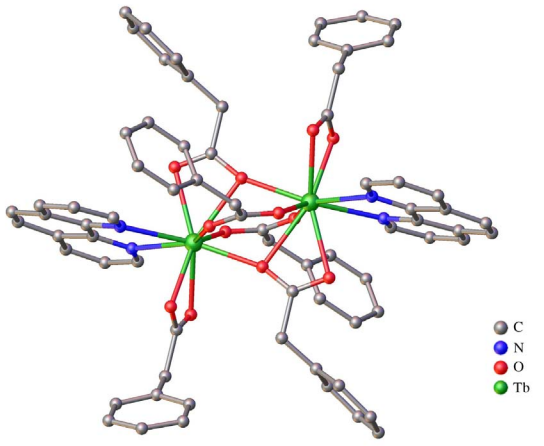

Figure 2 Structure of complex **2**. Hydrogen atoms are not shown.

for nonhydrogen atoms. The H atoms were added in the calculated positions and refined using the riding model in an isotropic approximation.

The polyhedron geometry was determined using the continuous shape measures (CShMs) and the SHAPE 2.1 program.[23] CShMs show the deviation of atom coordinates in the coordination environment of the metal ion from the vertices of ideal polyhedra. Full coincidence of the polyhedron geometry with the ideal shape corresponds to zero CShM.

Crystal data for **1**. $C_{68}H_{30}F_{20}N_4O_{12}Tb_2$ (M = 1792.80), T = 150 K, triclinic, space group $P\bar{1}$, a = 10.0950(7), b = 12.9881(16) and c = 13.1450(17) Å, α = 101.749(4)°, β = 105.232(3)°, γ = 106.265(3)°, V = 1523.2(3) Å^3, Z = 1, μ(MoKα) = 2.436 mm^{-1}. At the angles 2.00° < < 2θ < 29.00°, a total of 8992 reflections were measured, including 5807 unique reflections (R_{int} = 0.0339) and 4850 reflections with $I > 2\sigma(I)$, which were used in all calculations. The final R_1 = 0.0508, wR_2 = 0.0625 (all data) and R_1 = 0.0383, wR_2 = 0.0589 [$I > 2\sigma(I)$], GOOF = 0.981. Largest diff. peak/hole 0.782 and –0.955 eÅ^{-3}.

Crystal data for **2**. $C_{72}H_{58}N_4O_{12}Tb_2$ (M = 1489.06), T = 100 K, monoclinic, space group $P2_1/n$, a = 15.3098(11), b = 12.2732(9) and c = 16.4634(11) Å, β = 103.751(5)°, V = 3004.8(4) (10) Å^3, Z = 2, μ(CuKα) = 11.997 mm^{-1}. At the angles 3.545° < 2θ < 65.239°, a total of 30719 reflections were measured, including 5102 unique reflections (R_{int} = 0.1354) and 3520 reflections with $I > 2\ \sigma(I)$, which were used in all calculations. The final R_1 = 0.0970, wR_2 = 0.1303 (all data) and R_1 = 0.0573, wR_2 = 0.1154 [$I > 2\sigma(I)$], GOOF = 1.017. Largest diff. peak/hole 0.823 and –0.844 eÅ^{-3}.

Crystal data for **3**. $C_{70}H_{28}F_{30}N_4O_{14}Tb_2$ (M = 2036.80), T = 100 K, monoclinic, space group $P2_1/n$, a = 14.246(3), b = 15.606(2) and c = 16.711(3) Å, β = 109.148(7)°, V = 3509.7(11) Å^3, Z = 2, μ(MoKα) = 2.148 mm^{-1}. At the angles 2.092° < 2θ < 26.056°, a total of 24480 reflections were measured, including 6923 unique reflections (R_{int} = 0.0737) and 5092 reflections with $I > 2\sigma(I)$, which were used in all calculations. The final R_1 = 0.0690, wR_2 = 0.0709 (all data) and R_1 = 0.0392, wR_2 = 0.643 [$I > 2\sigma(I)$], GOOF = 1.022. Largest diff. peak/hole 0.825 and –1.669 eÅ^{-3}.

CCDC 2162021 (**1**), 2325960 (**2**) and 2309740 (**3**) contain the supplementary crystallographic data for this paper. These data can be obtained free of charge from The Cambridge Crystallographic Data Centre *via* http://www.ccdc.cam.ac.uk.

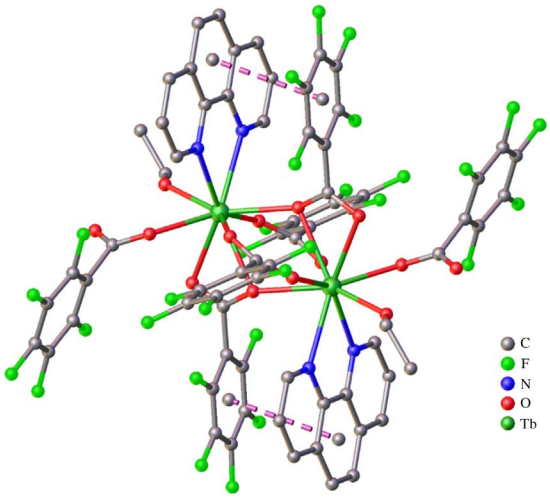

Figure 3 Structure of complex **3**. Intramolecular stacking interactions are indicated by dashed lines; hydrogen atoms are not shown.

distances between the centroids of aromatic fragments increased by 0.27 Å compared to that in compound **1** (Table S2). In contrast to compound **1**, intermolecular stacking interactions were absent from the crystal packing of **3**, and only intramolecular C–F···π, C–H···O, and C–H···F contacts and hydrogen bonds were observed (Tables S3, S4).

A Hirshfeld surface analysis was performed to identify the contribution of major non-covalent interactions in the packing of complexes **1**–**3**. The Hirshfeld surface in homoanionic complexes **2** and **3** was predominantly formed by O···H and C···H (in **2**) and C···F and H···F interactions (in **3**). In mixed carboxylate compound **1**, the primary contribution to the surface was made by F···H interactions with an observed increase in the contribution of C···C interactions and a decrease in the role of C···F and H···F interactions compared to complex **3** (Table S5).

The optical excitation spectra of luminescence for compounds **1**–**3** were measured at the wavelenth corresponding to the magnetic dipole transition of Tb^{3+} (547 nm) (Figure S5). Narrow bands at 380 and 489 nm were associated with $^7F_6$–$^5D_{2,3}$ and $^7F_6$–$^5D_4$ electronic transitions in the ion, respectively. Since intense wide bands at 300–360 nm correspond to electronic transitions within the ligand environment, the most effective luminescence of the complexes can be achieved upon excitation through the ligands. The photoluminescence spectra of crystalline powder compounds **1**–**3** were obtained upon excitation at 330 nm (Figure 4). The narrow bands at 490, 547, 586, 650, 670, and 680 nm originated from $^5D_4 \rightarrow {}^7F_J$ (J = 0–6) electronic $4f$–$4f^*$ transitions in the Tb^{3+} ion. There was no noticeable contribution

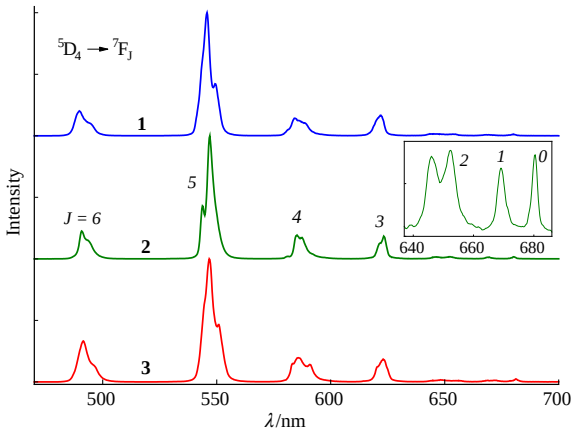

Figure 4 Photoluminescence spectra of compounds **1**–**3** recorded upon 330 nm excitation at room temperature.

Table 1 Photophysical parameters of compounds **1**–**3**: τ_1 and τ_2 are the lifetimes of excited states, A_1 and A_2 are the amplitude contributions of the observed temporal components, R^2 is adjusted root mean square error and Φ is the luminescence quantum yield estimated upon excitation at 330 nm.

Complex	τ_1/μs	τ_2/μs	A_1	A_2	R^2	Φ (%)
1	553.6 ± 3.2	1299.7 ± 1.2	0.20	0.80	0.999	60
2	219.4 ± 1.6	417.8 ± 1.1	0.32	0.67	0.999	12
3	1452.6 ± 0.2	–	0.99	–	0.999	64

from the ligand luminescence due to effective ligand-to-ion energy transfer. The emission band splitting was similar to that for comparable compounds with the low polyhedron symmetry.[24]

From the results of experiments, we determined that binuclear complexes with a perfluorinated ligand pfb (**1** and **3**) exhibited high quantum yields as the introduction of C–F oscillators into the ligand environment reduced the probability of non-radiative relaxation.[19]

Compared to complex **3**, compound **1** exhibited enhanced intramolecular stacking interactions and an increased contribution of intermolecular stacking interactions, which stabilized the crystal packing. This enhancement was attributed to aromatic phenylacetate anion fragments. In mixed carboxylate compound **1**, the lifetime and quantum yield of luminescence notably increased compared to those of phenylacetate complex **2**. However, when compared to pentafluorobenzoate complex **3**, the quantum yields were similar, and the lifetime of the excited state significantly decreased.

This work was supported by the Russian Science Foundation (grant no. 22-73-10192).

IR spectroscopy, X-ray diffraction, powder X-ray diffraction and CHN analyses of the complexes were performed using the equipment of the JRC PMR IGIC RAS as part of the state assignment of the IGIC RAS in the field of fundamental scientific research. Photophysical measurements were carried out with financial support from the Ministry of Science and Higher Education of the Russian Federation, using the equipment of the Research Center for Molecular Structure Studies, INEOS RAS.

Online Supplementary Materials

Supplementary data associated with this article can be found in the online version at doi: 10.1016/j.mencom.2024.06.005.

References

1 N. B. D. Lima, A. I. S. Silva, S. M. C. Gonçalves and A. M. Simas, *J. Lumin.*, 2016, **170**, 505.
2 A. D. Burrows, *CrystEngComm*, 2011, **13**, 3623.
3 Y. Kitagawa, M. Tsurui and Y. Hasegawa, *RSC Adv.*, 2022, **12**, 810.
4 N. B. D. Lima, S. M. C. Gonçalves, S. A. Júnior and A. M. Simas, *Sci. Rep.*, 2013, **3**, 2395.
5 J. K. Voronina, D. S. Yambulatov, A. S. Chistyakov, A. E. Bolot'ko, L. M. Efromeev, M. A. Shmelev, A. A. Sidorov and I. L. Eremenko, *Crystals*, 2023, **13**, 678.
6 M. A. Shmelev, J. K. Voronina, M. A. Evtyukhin, F. M. Dolgushin, E. A. Varaksina, I. V. Taydakov, A. A. Sidorov, I. L. Eremenko and M. A. Kiskin, *Inorganics*, 2022, **10**, 194.
7 A. S. Zaguzin, M. A. Bondarenko, P. A. Abramov, M. I. Rakhmanova, M. N. Sokolov, V. P. Fedin and S. A. Adonin, *Inorganics*, 2022, **10**, 262.
8 D. A. Bardonov, L. N. Puntus, I. V. Taidakov, E. A. Varaksina, K. A. Lyssenko, I. E. Nifant'ev and D. M. Roitershtein, *Mendeleev Commun.*, 2022, **32**, 198.
9 N. B. D. Lima, A. I. S. Silva, V. F. C. Santos, S. M. C. Gonçalves and A. M. Simas, *RSC Adv.*, 2017, **7**, 20811.
10 L. L. L. S. Melo, G. P. Castro, Jr. and S. M. C. Gonçalves, *Inorg. Chem.*, 2019, **58**, 3265.
11 J. S. Sidhu, R. P. Sharma, T. Aree and P. J. Venugopalan, *J. Fluorine Chem.*, 2009, **130**, 650.
12 R. P. Sharma, A. Saini, S. Singh, P. Venugopalan and W. T. A. Harrison, *J. Fluorine Chem.*, 2010, **131**, 456.

13 L. Li, H. Wang, W. Wang and W. J. Jin, *CrystEngComm*, 2017, **19**, 5058.
14 B. J. J. Timmer and T. J. Mooibroek, *J. Chem. Educ.*, 2021, **98**, 540.
15 H. R. Masoodi, R. S. Pourhosseini and S. Bagheri, *Comput. Theor. Chem.*, 2023, **1220**, 114022.
16 J. Pan, W. Lin, F. Bao, Q. Qiao, G. Zhang, Y. Lu and Z. Xu, *Chin. Chem. Lett.*, 2023, **34**, 107519.
17 M. A. Shmelev, Yu. K. Voronina, N. V. Gogoleva, M. A. Kiskin, A. A. Sidorov and I. L. Eremenko, *Russ. J. Coord. Chem.*, 2022, **48**, 224 (*Koord. Khim.*, 2022, **48**, 229).
18 M. A. Shmelev, G. N. Kuznetsova, N. V. Gogoleva, F. M. Dolgushin, Yu. V. Nelyubina, M. A. Kiskin, A. A. Sidorov and I. L. Eremenko, *Russ. Chem. Bull.*, 2021, **70**, 830.
19 J. Janczak, *J. Mol. Struct.*, 2020, **1207**, 127833.
20 G. M. Sheldrick, *SADABS*, Bruker AXS, Madison, WI, USA, 1997.
21 O. V. Dolomanov, L. J. Bourhis, R. J. Gildea, J. A. K. Howard and H. Puschmann, *J. Appl. Crystallogr.*, 2009, **42**, 339.
22 G. M. Sheldrick, *Acta Crystallogr.*, 2015, **C71**, 3.
23 D. Casanova, M. Llunell, P. Alemany and S. Alvarez, *Chem. – Eur. J.*, 2005, **11**, 1479.
24 X.-H. Wu, Y.-Y. Li, N. Ren and J.-J. Zhang, *ChemistrySelect*, 2018, **3**, 8003.

Received: 5th February 2024; Com. 24/7386